https://doi.org/10.5194/egusphere-2025-1533
Preprint. Discussion started: 7 May 2025

A new method for detecting aerosols: combining atmospheric detection LiDAR technology with intelligent driving technology

Hao Yang[1,2,3], Xiaomeng Zhu[1], Duoyang Qiu[1,2*], Xianyang Li[1], Zhiqiang Kuang[3],Zhiyuan Fang[5*], Yalin Hu[4,6]

[1]School of Advanced Manufacturing Engineering, Hefei University, Hefei 230601, China

[2]Anhui Provincial Engineering Technology Research Center of Intelligent Vehicle Control and Integrated Design Technology, Hefei University, Hefei 230601, China

[3]Hefei Innovation Institute, Hefei Institutes of Physical Science, Chinese Academy of Sciences, Hefei 230088, China

[4]University of Science and Technology of China, Hefei 230026, China

[5]School of Mechatronics and Energy Engineering, Ningbo Tech University, Ningbo 315100, China

[6]Anhui Institute of Optics and Fine Mechanics, Chinese Academy of Sciences, Hefei 230031, China

Corresponding author and email: Duoyang Qiu(qiudy@hfuu.edu.cn);
Zhiyuan Fang(fangzhy@mail.ustc.edu.cn)

Received: date; Accepted: date; Published: date

Abstract The existing aerosol mobile detection system has problems such as over-reliance on labor power and difficulty in conducting continuous operations in toxic and polluted environments. This paper presents a new method for detecting aerosols. The method combines atmospheric detection LiDAR technology and intelligent driving technology. Through modular design (including control module, aerosol detection module, environment sensing and positioning module, and wire control chassis module), an intelligent cruise detection system for aerosols was built. For path planning, Gaussian pseudo-spectrum method was used. The obstacle avoidance constraints and physical constraints during cruise detection movement was fully considered. Experiments were also conducted for three different application scenarios of continuous vertical detection, scanning detection and unmanned intelligent cruise detection. The experimental results show that the system can effectively and continuously acquire the vertical and spatial distribution of aerosol pollutants. It can achieve three-dimensional scanning and positioning tracking of atmospheric aerosols. It has the ability of unmanned cruise detection and real-time warning of regional pollution prevention and control. More detection experiments will be conducted in different environments in the future. We will continue to explore the application of this technology in intelligent cruise control, detection, and pollution prevention, providing new ideas for regional pollution monitoring.

Keywords: aerosol detection system, intelligent driving technology, LiDAR, regional pollution monitoring;

1. Introduction

Aerosols not only affect air quality (Monks et al., 2009), causing reduced visibility and leading to a

https://doi.org/10.5194/egusphere-2025-1533
Preprint. Discussion started: 7 May 2025

high incidence of traffic accidents(Gao et al., 2019), but also have an impact on climate(Kok et al., 2023). Some germs and viruses are spread by aerosols in the atmosphere. This poses a serious threat to public health and daily life.(Oh et al., 2020; Pope Iii, 2002).

Among the current means of aerosols detection, LiDAR has ultra-high sensitivity, good temporal and spatial resolution, and the ability to capture targets in three dimensions(Eitel et al., 2016). It provides all-weather monitoring of clouds, aerosols, and atmospheric constituents(Cairo et al., 2024), making it widely used for atmospheric environment detection. According to different platforms, it is divided into Space-borne LiDAR, airborne LiDAR and ground-based LiDAR. Large scale and multi latitude atmospheric data can be obtained through space-borne LiDAR, which can provide data for areas that are difficult to observe on the ground.(Chen et al., 2023; Sun et al., 2024). Some scholars have used aerosol products from Space-borne LiDAR to study dust transport processes and surface characterization(Song et al., 2024; Yang et al., 2025). However, the maintenance cost and technical requirements of Space-borne LiDAR are high, and it is impossible to achieve continuous detection of a certain area. Some researchers use airborne LiDAR to detect the distribution and concentration of marine aerosols(Eckert et al., 2024), while others use it to measure the optical characteristics of particulate matter(Girdwood, 2023). However, the high cost and airspace limitations have hindered the continued use of airborne LiDAR. Ground-based LiDAR is widely used to detect aerosol pollution. It can achieve continuous fixed-point detection and effectively monitor the vertical airspace over a specific area(Yang et al., 2024). LiDAR fixed on a building for continuous fixed-point vertical detection(Kuang et al., 2023), it's can capture of aerosol transport processes(Yang et al., 2021a). Zhang et al. used a ground-based lidar network to analyze a dust aerosol transport over northern China in 21 years(Zhang et al., 2024). LiDAR paired with a gimbal can carry out scanning detection. Horizontal scanning effectively captures contaminants within the detection distance. It enables pollutants to be effectively tracked and potential sources of contamination to be identified(Kuang et al., 2023). The cone scanning can detect the pollutants in the scanning area by stereoscopic scanning and provide strong data support(Xie et al., 2015). If ground-based LiDAR is mounted on a mobile platform, navigation detection can be achieved. It has the advantages of large detection range and long detection distance, and can perform large-scale mobile detection in urban areas.(Wang et al., 2024). It is even possible to observe the optical characterization of pollutants in a geographic area on a continuously moving basis and to detect sources of pollution(Lv et al., 2017; Wang et al., 2009).

However, the need for uninterrupted cruise detection during regional pollution prevention and control actions, which can lead to a significant loss of operator energy. This has resulted in a significant increase in labor costs for existing manned cruise detection systems. In addition, being in an environment with high concentrations of toxic pollutant emissions can cause irreversible damage to the bodies of researchers. In order to address the above issues. This paper presents a new method for detecting aerosols.

https://doi.org/10.5194/egusphere-2025-1533
Preprint. Discussion started: 7 May 2025

The method combines atmospheric detection LiDAR technology and intelligent driving technology. The system can carry out unmanned cruise detection for long periods of time, providing a new way of thinking about regional pollutant monitoring. The second part introduces the system and research method. The third part analyzes the results of different experiments. The fourth part is summary and prospect.

2. Systems and research method

2.1 System Principles and Models

Intelligent cruise detection system for aerosols is shown in Fig. 1. The system comprises a control module, an aerosol detection module, an environment sensing and positioning module, and a wire control chassis module, and is integrated into a small electric unmanned vehicle. The control module is composed of industrial controller, vehicle controller and gateway. The environment sensing and positioning module includes vehicle LiDAR, millimeter-wave radar, binocular camera, and an integrated navigation system (including GPS antenna and inertial navigation). The wire control chassis module consists of brake module, drive module and steering module.

As the "brain" of the whole system, the control module controls the operation of the whole system. The industrial controller receives the localization data and environmental data detected by the environment awareness and localization module through the processing gateway. Based on this input, it’s dynamically computing the required gear ratio, velocity parameters, and braking force for the unmanned vehicle and transmits these values via the vehicle controller to the wire control chassis module. The wire control chassis module feeds back the state of the moving vehicle parameters (speed, acceleration, rotational speed and braking, etc.) to the industrial controller. The detection LiDAR in the aerosol detection module is a Mie-scattering LiDAR. The Mie-scattering LiDAR communicates with the industrial computer via a router. Fig.1b is the module distribution of the detection system. Mie-scattering LiDAR placed on the roof of an unmanned vehicle. The unmanned vehicle is equipped with a 220V inverter to provide a stable power supply for the Mie-scattering LiDAR and the industrial controller. The relevant technical parameters of the system can be seen in Table 1.

https://doi.org/10.5194/egusphere-2025-1533
Preprint. Discussion started: 7 May 2025

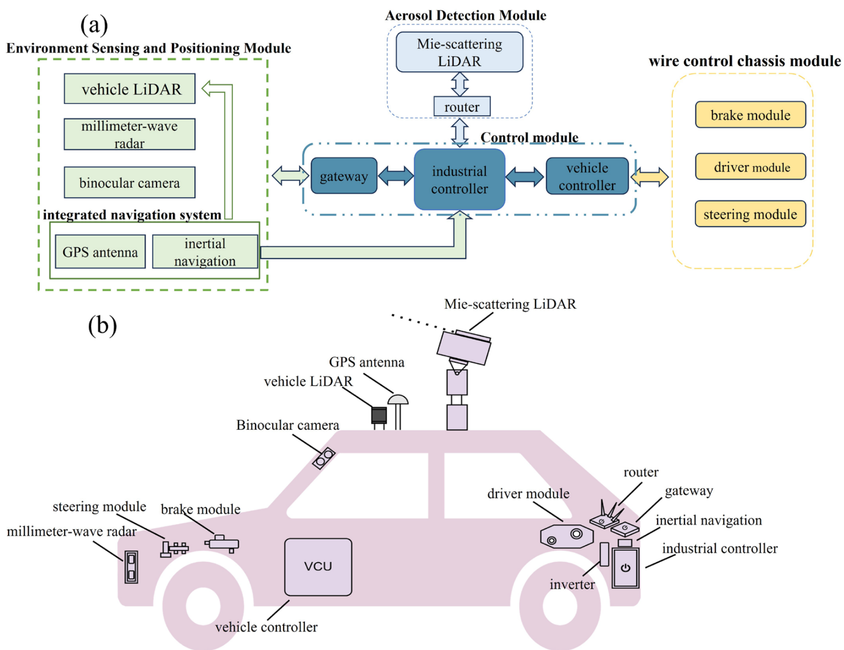

Fig. 1 Intelligent cruise detection system for aerosols; (a) shows the system schematic; (b) shows the system module distribution (this figure is an original creation by the authors).

Table 1 Relevant technical parameters of Intelligent cruise detection system for aerosols

	parameters	numerical value
Mie-scattering LiDAR Technical Parameters	laser wavelength	1064nm
	pulse energy	15μJ
	Pulse Repetition Frequency	10kHz
	Acquisition Channel	1800
	Distance resolution	7.5m
Unmanned Vehicle Technical Parameters	Wheelbases(L)	2.56m
	Vehicle front overhang(f)	0.902m
	Vehicle rear overhang(r)	0.883m
	body width(d)	1.765m

https://doi.org/10.5194/egusphere-2025-1533
Preprint. Discussion started: 7 May 2025

2.2 Aerosol detection methods

Mie-scattering LiDAR is commonly used to measure dust aerosols, and the equation of LiDAR is(Megie, 1985; Yang et al., 2021b):

$$P(z) = (C[\beta_m(z) + \beta_a(z)] * exp\{-2\int_0^z [\alpha_m(z') + \alpha_a(z')]dz'\}) / z^2 \tag{1}$$

In the formula (1), *P(z)* is the received echo signal of height z, C is the LiDAR constant. βm and βa are the backscattering coefficients of atmospheric molecules and aerosols respectively. α_m and α_a are the extinction coefficients of atmospheric molecules and aerosol molecules, respectively. z is the height of aerosol LiDAR detection.

In order to make the detection results more accurate, the range-corrected signal is usually used:

$$X = P(z) * z^2 \tag{2}$$

Previous studies have indicated that aerosols with more pronounced non-spherical characteristics tend to exhibit higher depolarization ratios. The equation for the depolarization ratio is (Urbanek et al., 2018)：

$$\delta_{(z)} = k\frac{P_s(z)}{P_p(z)} \tag{3}$$

In the formula (3), δ(z)represents the depolarization ratio, k is the gain constant ratio, Ps (z) and Pp (z)represents the vertical and parallel components of atmospheric backscattered echo power at height z, respectively.

2.3 Unmanned Vehicle Obstacle Avoidance Constraints

Unmanned vehicles need to satisfy their own physical and mechanical constraints while traveling. This is translated into inequality constraints on some of the state and control variables as follows:

$$\begin{cases} |\mathrm{v(t)}| \leq \mathrm{v}_{\max} \\ |\mathrm{a(t)}| \leq \mathrm{a}_{\max} \\ |\mathrm{j(t)}| \leq \mathrm{j}_{\max} \quad ,t \in [t_0, t_f] \\ |\varphi(t)| \leq \varphi_{\max} \\ |\omega(t)| \leq \omega_{\max} \end{cases} \tag{4}$$

In Formula (4),V_{max} is the maximum permissible speed during driving. a_{max} is the maximum acceleration allowed during driving. j_{max} is the maximum rate of change of acceleration allowed during driving. φ_{max} is the maximum allowable front wheel equivalent swing angle. ω_{max} is the maximum allowable front wheel swing angle angular velocity.

https://doi.org/10.5194/egusphere-2025-1533
Preprint. Discussion started: 7 May 2025

Vehicle collision avoidance constraints are important when solving trajectory planning problems. The actual top-view projection shape of the vehicle is close to a rectangle. Here the vehicle contour is depicted with an enlarged rectangle. d_{safe} is the safety threshold to ensure that the vehicle is collision free.

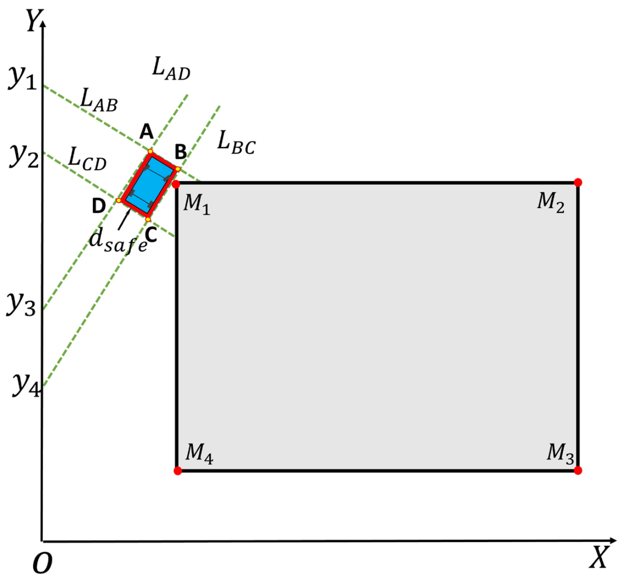

Fig. 2 Schematic diagram of obstacle avoidance constraints.

As shown in Fig. 2. The red area around the vehicle is the safety threshold to ensure a collision-free vehicle. If the vehicle does not collide with point M while traveling, the point *M* coordinates are always outside the rectangular *ABCD* region. Remember that the four sides of the rectangle are the lines L_{AB}, L_{BC}, L_{CD}, and L_{AD}, and their linear equations are as follows:

$$\begin{cases} L_{AB} = k_1 * x + y_1 \\ L_{CD} = k_1 * x + y_2 \\ L_{AD} = k_2 * x + y_3 \\ L_{BC} = k_2 * x + y_4 \end{cases} \tag{5}$$

k_1 is the slope of the lines L_{AB}, and L_{CD}, k_2 is the slope of the lines L_{AD}, and L_{BC}. If the line L_{AB} is parallel or perpendicular to the X-axis so that the point *M* is outside the rectangle *ABCD*, then the coordinates of the point M must satisfy the following conditions:

$$\begin{cases} M_{ix} < D_x(t) OR M_{ix} > A_x(t) OR M_{iy} < C_y(t) OR M_{iy} > A_y(t), \theta = 0^{\circ} \\ M_{ix} < D_x(t) OR M_{ix} > C_x(t) OR M_{iy} < D_y(t) OR M_{iy} > A_y(t), \theta = 90^{\circ} \\ M_{ix} < A_x(t) OR M_{ix} > D_x(t) OR M_{iy} < D_y(t) OR M_{iy} > C_y(t), \theta = 180^{\circ} \\ M_{ix} < D_x(t) OR M_{ix} > C_x(t) OR M_{iy} < A_y(t) OR M_{iy} > D_y(t), \theta = 270^{\circ} \end{cases} \tag{6}$$

https://doi.org/10.5194/egusphere-2025-1533
Preprint. Discussion started: 7 May 2025

where 1, 2, 3, and 4 represent the four vertices of the rectangle.

When the line L_{AB} is not parallel or perpendicular to the X-axis, if the point M is outside $ABCD$. The following conditions must be satisfied:

$$\begin{cases} (M_{iy} - k_1 * M_{ix}) < y_2 OR (M_{iy} - k_1 * M_{ix}) > y_1 \\ (M_{iy} - k_2 * M_{ix}) < y_4 OR (M_{iy} - k_2 * M_{ix}) > y_3 \end{cases} \tag{7}$$

2.4 Unmanned Mobile Detection Path Planning and Simulation

The Bolza problem for nonlinear optimal control can be described as:

$$\min \psi = \phi(\xi(t_0), t_0, \xi(t_f), t_f) + \int_{t_0}^{t_f} g(\xi(t), \mu(t), t) dt \tag{8}$$

In the formula (8): $\xi(t)$ and $\mu(t)$ are the state and control variables of the system, respectively, $\xi(t) \in R^n$ and $\mu(t) \in R^m$ satisfy . t_0 and t_f are the initial and termination moments respectively, for the objective function of the optimal control problem.

$$s.t. \begin{cases} \dot{\xi}(t) = f(\xi(t), \mu(t), t) \\ M(\xi(t), \mu(t), t) \le 0 \qquad t \in [t_0, t_f] \\ N(\xi(t_0), t_0, \xi(t_f), t_f) = 0 \end{cases} \tag{9}$$

In the formula (9): The first behavior describes the differential equation of state of the system. The second behavior is an inequality constraint on the system variables during the solution of the objective function. The third behavior is an equational constraint on the system variables during the solution of the objective function. Trajectory planning for vehicles is actually a generalized Bolza problem for nonlinear optimal control.

In this paper, the segmented Gaussian pseudo-spectral method was used, which has the advantages of faster convergence and high success rate of solution. Gaussian pseudo-spectral method is a direct method for solving nonlinear optimal control problems. The method constructs Lagrange interpolation polynomials to approximate the state and control variables after discretizing the continuous optimization problem at the Legendre-Gauss (LG) collocation point. And replace the differential equation constraints with algebraic constraints, thus transforming the optimal control problem into a Nonlinear Programming (NLP) problem to be solved. Qiu et al. proposed a hierarchical trajectory planning and tracking control algorithm for unmanned vehicles combining Model Predictive Control (MPC) and Gaussian Pseudo-spectral Method (GPM). (Qiu et al., 2021).

The unmanned cruise detection experiment was chosen near one of the laboratory buildings. See Table 1 for unmanned vehicle parameters. The physical constraints are shown in Table 2. Fig. 3 shows the validation and simulation analysis of the trajectory planning algorithm based on the Gaussian pseudo-spectral method. The results show that obstacle avoidance can be achieved during cruise detection. And

https://doi.org/10.5194/egusphere-2025-1533
Preprint. Discussion started: 7 May 2025

plan paths according to the experimental roads to ensure safe and normal cruising.

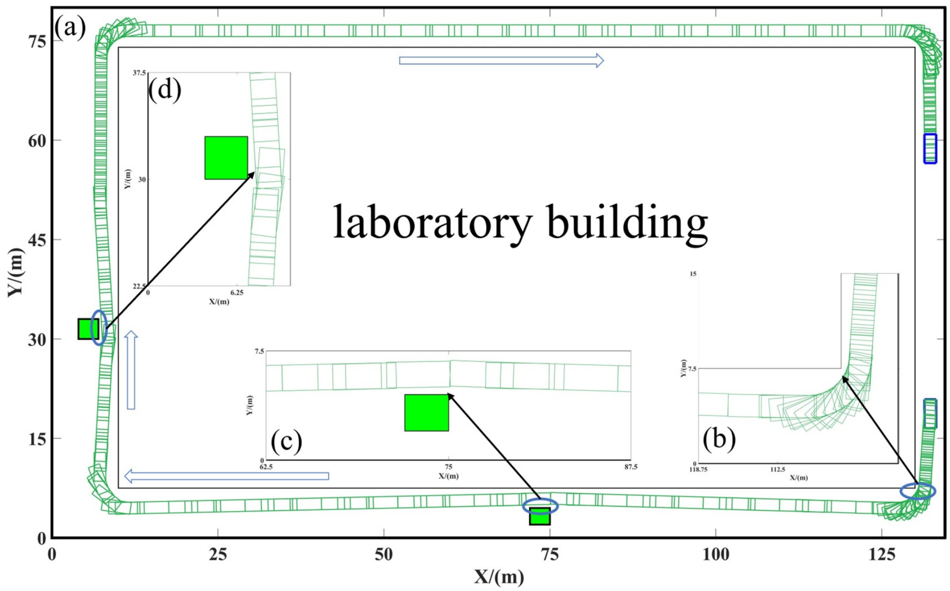

Fig. 3 Simulation of Cruise Detection Path Planning；(b), (c) and (d) show the simulation of obstacle avoidance for cornering, obstacle 1 and obstacle 2, respectively.

Table 2 Physical constraints for unmanned vehicles

Physical Constraints for Unmanned Vehicles					
parameters	V_{max}	a_{max}	j_{max}	φ_{max}	ω_{max}
numerical value	1.0m/s	0.1m/s^2	0.5m/s^3	0.56rad	0.56rad/s

3 Experimental results and analysis

3.1 Vertical Detection

We carried out an outdoor fixed point continuous detection on February 24, 2025. Fig. 4a shows the Range-corrected signal data of that day. Fig. 4b shows the depolarization ratio data. The Range-corrected signal can indicate the change in aerosol pollutant concentration on the same day. The depolarization ratio shows the non-spherical characteristics of aerosol pollutants. In Fig 4a, the temporal evolution of the vertical distribution of the near-surface aerosol layer is illustrated. The height of the aerosol layer was maintained at about 1.5 km for a long period of time. The pollution concentration value decreases with the change of time from about 0.7 $W\cdot km^2$ to 0.2 $W\cdot km^2$~0.3 $W\cdot km^2$. Clouds were also detected at 2km to

https://doi.org/10.5194/egusphere-2025-1533
Preprint. Discussion started: 7 May 2025

2.5km. Stratification of the depolarization ratio was observed between 00:00 and 05:00 on the 24th, as illustrated in Fig. 4b. The height of stratification gradually decreases until it disappears. The lower value is maintained around 0.2; the upper layer value is larger, reaching 0.9~1.1. This suggests that there is an input of exogenous coarse particulate aerosol and gradual deposition to merge with the local fine particulate matter. After 6 o 'clock, the foreign coarse particles and local fine particles were fully fused, and the depolarization ratio value was maintained between 0.8 and 1. The depolarization ratio reaches a maximum of 1.4 at around 10:00. The value of the receding polarization ratio gradually decreases to about 0.5 after 16:00, indicating that the coarse particulate pollutants have diffused away.

In order to verify the accuracy of the system's detection, we also selected the hourly particulate matter concentration observed at the ground station in Hefei City on February 24th. Fig. 4c shows the change curves of $PM_{2.5}$, PM_{10} and $PM_{2.5}/PM_{10}$ concentrations on that date. $PM_{2.5}$ and PM_{10} concentrations were higher than 100μg/m^3 from 0:00 to 5:00. $PM_{2.5}/PM_{10}$ values were around 0.8, indicating that the pollution in this phase is local fine particulate matter. Both concentrations then declined rapidly reaching a minimum at 10:00(56μg/m^3 for PM_{10} and 23μg/m^3 for $PM_{2.5}$). However, $PM_{2.5}/PM_{10}$ values also dropped to 0.4, indicating that coarse particulate matter dominated at this time. At 16:00, the subsequent concentrations all rebounded, and the $PM_{2.5}/PM_{10}$ value stabilized between 0.5 and 0.6. Fig. 4 illustrates that the pollution that caused the 24th was a mixture of local fine particulate pollutants and foreign coarse particulate aerosol pollutants. It was verified that the system is capable of observing the causes of aerosol pollution and its changes over the region.

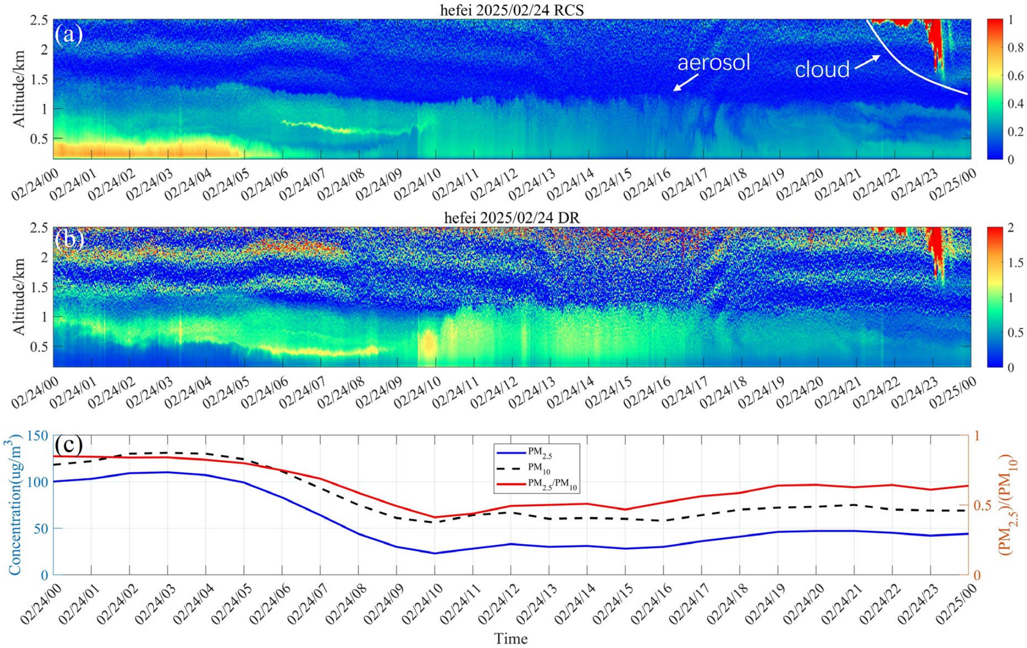

https://doi.org/10.5194/egusphere-2025-1533
Preprint. Discussion started: 7 May 2025

Fig. 4 Temporal variations in pollutant on 24 February; (a)and (b) are the Range-corrected signal (W·km²) and the depolarization ratio obtained from Mie-scattering LiDAR respectively;(c) is the concentration of particulate matter at the ground station (blue line indicates $PM_{2.5}$, black line segment indicates PM_{10}, and red line indicates $PM_{2.5}/PM_{10}$).

3.2 Cone-Scanning Detection

We conducted cone-scanning detection experiments on February 28, March 5, and March 6, 2025, respectively. The 0° direction is due west and the pitch angle is 75°, and the Range-corrected data were optioned for a range of 2.5 km. Fig. 5 shows the Range-corrected signal of cloudy days (February 28), polluted days (March 5) and clean days (March 6). From the Fig.5.We can see the presence of clouds at 1.7km to the southeast (180°~240°) on the 28th, and the presence of aerosol air masses at about 0.67km at the point with a small concentration. Thin clouds were distributed near the ground (around 0.85km) on the 5th. Compared with the other two days, the aerosol air mass at the location on the 5th was widely distribute. The system can achieve three-dimensional scanning and positioning tracking of atmospheric aerosols.

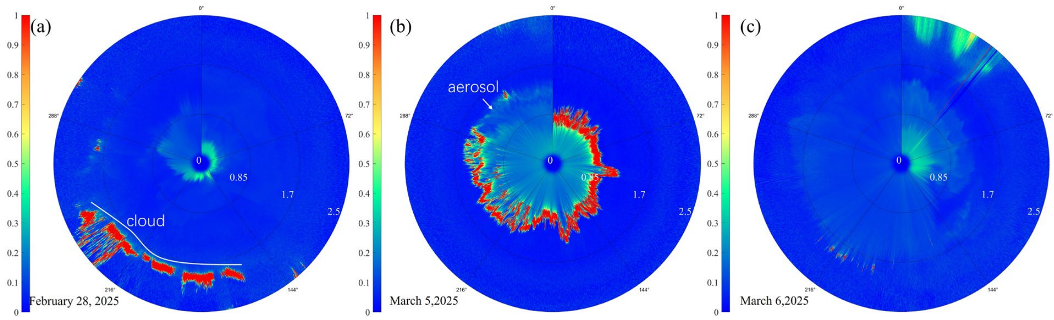

Fig. 5 Range-corrected signal(W·km²) from cone-scanning detection；(a) for February 28, 2025; (b) for March 5, 2025; and (c) for March 6, 2025.

3.3 Unmanned Intelligent Cruise Detection

We did an unmanned intelligent cruise detection experiment on February 26th. The location of the experiment was chosen near a laboratory building within the school. Before the experiment, enter the Mie-scattering LiDAR system to configure the relevant detection parameters. This is followed by turning on the wire control chassis module of the unmanned vehicle and the modules related to the environment sensing and positioning module. Finally, the planned path is selected and the vehicle switches to autopilot.

Fig. 6 shows a plot of the Range-corrected signal from one unmanned cruise detection. On the day of the experiment, the air status index (AQI) of Hefei was 115, $PM_{2.5}$ was 80μg/m^3, and PM_{10} was 1
0
0
μ
g

https://doi.org/10.5194/egusphere-2025-1533
Preprint. Discussion started: 7 May 2025

0.5 km in the later stages of the experiment. The results show that the system has the ability of unmanned cruise detection and real-time warning of regional pollution prevention and control.

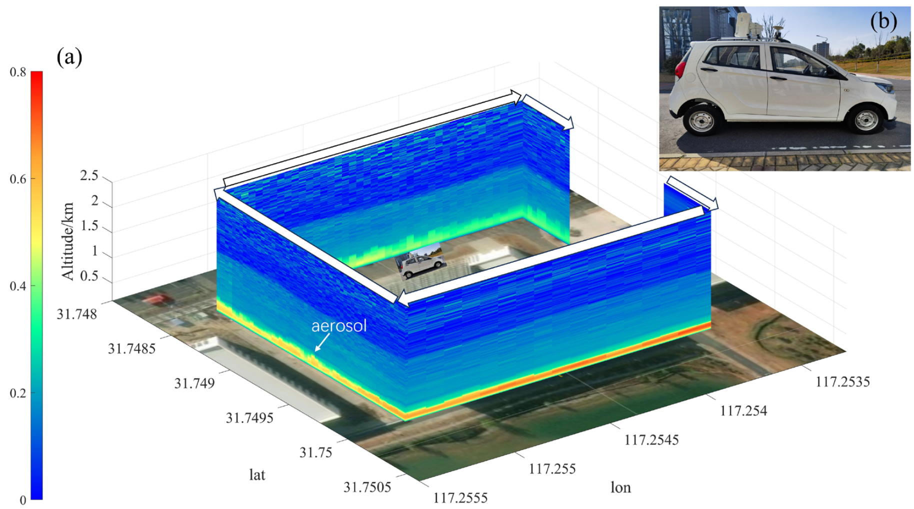

Fig. 6 Range-corrected signal (W·km²) superimposed on the map；(a) is a map of Range-corrected signal for unmanned move detection (arrows are in the direction of vehicle travel); (b) is an unmanned vehicle undergoing an unmanned walking experiment. (The map is a simple block map, ©2025Baidu-GS(2023)3206.)

4 Conclusions and outlook

We propose a new approach to aerosol detection that combines atmospheric detection LiDAR technology and smart driving technology. The intelligent cruise detection system for aerosols was built through a modularized design. The system includes: a control module, an aerosol detection module, an environment sensing and positioning module, and a wire control chassis module. Firstly, continuous vertical detection experiments show that the system can continuously observe the vertical distribution and depolarization ratio of aerosols for a long time (24 hours). And it can provide the fine structure of clouds and aerosols from 0-2.5km. The causes and changes of aerosol pollution over the detection area can be obtained through analysis. In addition, through scanning detection, the system has long-term 0-360° scanning detection capability. The system is capable of effective detection of different weather conditions (clean, polluted and cloudy days). Finally, an unmanned intelligent cruise detection experiment is conducted. The results of the experiment showed that the aerosol height increased from 0.3km to 0.5km on the day of the experiment and the pollution concentration gradually decreased from 0.8 W·km² to about 0.2 W·km². It shows that the system is capable of stable unmanned cruise detection and has ability to monitor the concentration and spatial distribution of pollutants. Experimentally

https://doi.org/10.5194/egusphere-2025-1533
Preprint. Discussion started: 7 May 2025

demonstrated in three different ways: the system can obtain the vertical and spatial distribute on of aerosol pollutants effectively and continuously; it can achieve three-dimensional scanning and positioning tracking of atmospheric aerosols; it has the capability of unmanned cruise detection and real-time warning of regional pollution prevention and control.

Our team realized multi-sensor fusion. The safety and effectiveness of this method are verified by the experiments of three application scenarios in the park. In the future, we will expand the scope of the detection area and conduct different detection experiments for different pollution scenarios. Intelligent cruise detection for complex scenes will also be further optimized in our subsequent long-term experiments. We will continue to explore the application of relevant technologies in intelligent cruise, detection and pollution prevention, and provide new ideas for regional pollution monitoring.

Declaration of Competing Interest

The authors declare no conflict of interest.

Data availability

The LiDAR data presented in this study are available from the corresponding author upon request(yh9599@mail.ustc.edu.cn). Particulate matter concentration data from China Environmental Monitoring Station for providing the particulate matter data(**http://106.37.208.233:20035**).

Financial support

This work is jointly funded by the National Science Foundation of China (Grant No. 42405069), the University Natural Sciences Research Project of Anhui Province (Grant No. 2023AH052201 and 2023AH052184), the 2023Talent Research Fund Project of Hefei University (No.23RC01), and the Technical Development Project of Hefei University (No.902/22050124128, No.902/22050124148, No.902/22050124149, and No.902/22050124250).

Author Contributions

Supervision, Hao Yang; designed the study, Xiaomeng Zhu; Methodology, Xiaomeng Zhu; Software, Hao Yang and Zhiqiang Kuang, Duoyang Qiu, Zhiyuan Fang; Xiaomeng Zhu and Xianyang Li; Writing–original draft, Xiaomeng Zhu; Writing–review & editing, Yalin Hu, Zhiyuan Fang, Xiaomeng Zhu, Xianyang Li, Duoyang Qiu and Hao Yang.

Reference

https://doi.org/10.5194/egusphere-2025-1533
Preprint. Discussion started: 7 May 2025

Monks, P.S., Granier, C., Fuzzi, S., Stohl, A., Williams, M.L., Akimoto, H., Amann, M., Baklanov, A., Baltensperger, U., Bey, I., Blake, N., Blake, R.S., Carslaw, K., Cooper, O.R., Dentener, F., Fowler, D., Fragkou, E., Frost, G.J., Generoso, S., Ginoux, P., Grewe, V., Guenther, A., Hansson, H.C., Henne, S., Hjorth, J., Hofzumahaus, A., Huntrieser, H., Isaksen, I.S.A., Jenkin, M.E., Kaiser, J., Kanakidou, M., Klimont, Z., Kulmala, M., Laj, P., Lawrence, M.G., Lee, J.D., Liousse, C., Maione, M., McFiggans, G., Metzger, A., Mieville, A., Moussiopoulos, N., Orlando, J.J., O'Dowd, C.D., Palmer, P.I., Parrish, D.D., Petzold, A., Platt, U., Pöschl, U., Prévôt, A.S.H., Reeves, C.E., Reimann, S., Rudich, Y., Sellegri, K., Steinbrecher, R., Simpson, D., Ten Brink, H., Theloke, J., Van Der Werf, G.R., Vautard, R., Vestreng, V., Vlachokostas, Ch., Von Glasow, R. Atmospheric composition change – global and regional air quality. Atmospheric Environment 2009.43, 5268–5350. https://doi.org/10.1016/j.atmosenv.2009.08.021

Gao, K.; Tu, H.; Shi, H. Stage-Specific Impacts of Hazy Weather on Car Following. Proceedings of the Institution of Civil Engineers - Transport 2019, 172 (6), 347–359. https://doi.org/10.1680/jtran.16.00182.

Kok, J. F.; Storelvmo, T.; Karydis, V. A.; Adebiyi, A.; Mahowald, N. M.; Evan, A. T.; He, C.; Leung, D. M. Mineral Dust Aerosol Impacts on Global Climate and Climate Change.

Oh H, Ma Y, Kim J. Human Inhalation Exposure to Aerosol and Health Effect: Aerosol Monitoring and Modelling Regional Deposited Doses[J]. International Journal of Environmental Research and Public Health,2020,17(6).

III P A C, Burnett T R, Thun J M, et al. Lung Cancer, Cardiopulmonary Mortality, and Long-Term Exposure to Fine Particulate Air Pollution. JAMA 2002, 287 (9), 1132. https://doi.org/10.1001/jama.287.9.1132.

Eitel, J.U.H., Höfle, B., Vierling, L.A., Abellán, A., Asner, G.P., Deems, J.S., Glennie, C.L., Joerg, P.C., LeWinter, A.L., Magney, T.S., Mandlburger, G., Morton, D.C., Müller, J., Vierling, K.T. Beyond 3-D: The new spectrum of lidar applications for earth and ecological sciences. Remote Sensing of Environment 186, 372–392. https://doi.org/10.1016/j.rse.2016.08.018

Cairo, F.; Di Liberto, L.; Dionisi, D.; Snels, M. Understanding Aerosol–Cloud Interactions through Lidar Techniques: A Review. Remote Sensing 2024, 16 (15), 2788. https://doi.org/10.3390/rs16152788.

Sun, K.; Dai, G.; Wu, S.; Reitebuch, O.; Baars, H.; Liu, J.; Zhang, S. Effect of Wind Speed on Marine Aerosol Optical Properties over Remote Oceans with Use of Spaceborne Lidar Observations. *Atmospheric Chemistry and Physics* **2024**, *24* (7), 4389–4409.

Chen, W.; Liu, J.; Hou, X.; Zang, H.; Wan, Y.; Zhu, X.; Ma, X.; Chen, D.; Li, R. Spaceborne Aerosol and Carbon Dioxide Detection Lidar (ACDL) Status and Progress; Springer, 2023; pp 97–107.

Yang, H.; Zhu, X.; Qiu, D.; Fang, Z.; Hu, Y.; Li, X. Research of Two Dust Transport Pollution in Northern China in 2023: Perspectives from LiDAR and Multi Source Data. Atmospheric Pollution Research 2025, 102441.

Song, Rui, Adam Povey, and Roy G Grainger, 'Characterization of Dust Aerosols from ALADIN and CALIOP Measurements', *Atmospheric Measurement Techniques*, 17.8 (2024), pp. 2521–38

Eckert, C.; Hernandez-Jaramillo, D. C.; Medcraft, C.; Harrison, D. P.; Kelaher, B. P. Drone-Based Measurement of the Size Distribution and Concentration of Marine Aerosols above the Great Barrier Reef. Drones 2024, 8 (7), 292.

Girdwood, J. Optical Measurement of Airborne Particles on Unmanned Aircraft. **2023**.

Yang, H.; Zhu, X.; Fang, Z.; Qiu, D.; Hu, Y.; Tian, C.; Ming, F. Study on the Vertical Distribution and Transport of Aerosols in the Joint Observation of Satellite and Ground-Based LiDAR. *Atmosphere* **2024**, *15* (2), 240. https://doi.org/10.3390/atmos15020240.

Kuang, Z.; Liu, D.; Wu, D.; Wang, Z.; Li, C.; Deng, Q. Parameter Optimization and Development of Mini Infrared Lidar for Atmospheric Three-Dimensional Detection. *Sensors* **2023**, *23* (2), 892. https://doi.org/10.3390/s23020892.

Yang, H.; Fang, Z.; Cao, Y.; Xie, C.; Zhou, T.; Wang, B.; Xing, K.; Lolli, S. Impacts of Transboundary Dust Transport on Aerosol Pollution in the Western Yangtze River Delta Region, China: Insights Gained From Ground-Based Lidar and Satellite Observations. *Earth and Space Science* **2021**, *8* (3), e2020EA001533. https://doi.org/10.1029/2020EA001533.

Zhang, Z.; Kuang, Z.; Yu, C.; Wu, D.; Shi, Q.; Zhang, S.; Wang, Z.; Liu, D. Trans-Boundary Dust Transport of Dust Storms in Northern China: A Study Utilizing Ground-Based Lidar Network and CALIPSO Satellite. *Remote Sensing* **2024**, *16* (7), 1196. https://doi.org/10.3390/rs16071196.

Xie, C.; Zhao, M.; Wang, B.; Zhong, Z.; Wang, L.; Liu, D.; Wang, Y. Study of the Scanning Lidar on the Atmospheric Detection. *Journal of Quantitative Spectroscopy and Radiative Transfer* **2015**, *150*, 114–120. doi:10.1016/j.jqsrt.2014.08.023

Wang, Y.; Wang, H.; Qin, Y.; Xu, X.; He, G.; Liu, N.; Miao, S.; Lu, X.; Wang, H.; Fan, S. Measurement Report: Nocturnal Subsidence behind the Cold Front Enhances Surface Particulate Matter in Plains Regions: Observations from the Mobile Multi-Lidar System. *Atmos. Chem. Phys.* **2024**, *24* (4), 2267–2285. https://doi.org/10.5194/acp-24-2267-2024.

Lv, L.; Liu, W.; Zhang, T.; Chen, Z.; Dong, Y.; Fan, G.; Xiang, Y.; Yao, Y.; Yang, N.; Chu, B. Observations of Particle Extinction, PM2. 5 Mass Concentration Profile and Flux in North China Based on Mobile Lidar Technique. *Atmospheric Environment* **2017**, *164*, 360–369.

Wang, M.; Zhu, T.; Zheng, J.; Zhang, R. Y.; Zhang, S. Q.; Xie, X. X.; Han, Y. Q.; Li, Y. Use of a Mobile Laboratory to Evaluate Changes in On-Road Air Pollutants during the Beijing 2008 Summer Olympics. *Atmos. Chem. Phys.* **2009**.

https://doi.org/10.5194/egusphere-2025-1533
Preprint. Discussion started: 7 May 2025

Megie, G., 1985. *Laser Remote Sensing: Fundamentals and Applications*. Wiley, New York.

Yang, H.; Zhu, X.; Fang, Z.; Qiu, D.; Hu, Y.; Tian, C.; Ming, F. Study on the Vertical Distribution and Transport of Aerosols in the Joint Observation of Satellite and Ground-Based LiDAR. *Atmosphere* **2024**, *15* (2), 240. https://doi.org/10.3390/atmos15020240.

Urbanek, B.; Groß, S.; Wirth, M.; Rolf, C.; Krämer, M.; Voigt, C. High Depolarization Ratios of Naturally Occurring Cirrus Clouds Near Air Traffic Regions Over Europe. *Geophysical Research Letters* **2018**, *45* (23). https://doi.org/10.1029/2018GL079345.

Qiu, D.; Qiu, D.; Wu, B.; Gu, M.; Zhu, M. Hierarchical Control of Trajectory Planning and Trajectory Tracking for Autonomous Parallel Parking. *IEEE Access* **2021**, *9*, 94845–94861. doi:10.1109/ACCESS.2021.3093930